

# Flow Separation Characteristics of a Thrust Optimized Parabolic Nozzle in a High Altitude Simulation Chamber

S.B.Verma\*

Research Scientist, Experimental Aerodynamics Division (EAD),  
National Aerospace Laboratories (CSIR), Bangalore, INDIA

Oskar Haidn<sup>#</sup>

Vice-Director and Head of Technology, Institute of Space Propulsion,  
German Aerospace Center, DLR Lampoldshausen, GERMANY

**Abstract:** An experimental investigation has been carried out to study the effect of high altitude chamber testing on the flow structure and the associated side-load development in a thrust optimized parabolic nozzle. It is observed that the normal shock location for tests in SEM is located downstream of its position in sea-level case. The incipient separation location in SEM is also found to be considerably upstream of its location under sea-level tests. The above changes cause the momentum imbalance along the overexpansion and reflected shocks to only favor FSS condition (both during start up and shut down) and hence, flow transitions such as FSS to pRSS or RSS and *vice-versa* are totally prevented. Although not conclusive at this moment, the primary cause responsible for the observed flow conditions seems to be the reduced mass flow required to attain similar NPR inside a HASC which prevents nitrogen condensation and hence, affects the flow development inside a TOP nozzle. The increase in wall pressure fluctuations and the side-load signal between the NPR of side-load peaks in SEM suggests interference effects between the nozzle exhaust and the diffuser.

## I. Introduction

Flow separation in high expansion nozzles during sea-level operation, such as transient start up and shut down, is inevitable and occurs through a separation shock. The flow unsteadiness associated with the separation shock in combination with any flow asymmetry can generate dangerous side-loads. The occurrence of side-loads puts constraints on the overall performance-to-weight ratio of the nozzle and hence, flow separation and the associated side-loads in rocket nozzles, have been the subject of research, both experimentally and numerically. Initially, Nave and Coffey [1] during the Apollo developmental program in 1970, observed from their cold tests of the subscale J-2S engine that flow reattachment downstream of separation can occur leading to dangerous lateral forces. Intense side-load activity has also been reported in the rocket nozzles of most high performance engines such as the SSME and Vulcain engine (parabolic contour), LE-

---

\* Nozzle Flow Group, EAD, NAL Bangalore, India, E-Mail: [sbverma@ead.cmmacs.ernet.in](mailto:sbverma@ead.cmmacs.ernet.in)

# Vice Director and Head of Technology, DLR Lampoldshausen, E-Mail: [oskar.haidn@dlr.de](mailto:oskar.haidn@dlr.de)

7A engine (CTP contour) (H-IIA) and on LR-115 (Saturn C-1), Viking (Ariane 4) and RD-0120 engine (Russian Energia Launcher)) using TIC design.

The main engines of present day parallel-stage launch vehicles usually use a thrust optimized parabolic (TOP) nozzle primarily because of their high thrust-to-mass ratio. The exhaust flow from such nozzles feature an internal shock that originates slightly downstream of the point (at the beginning of the divergent section) where the wall contour undergoes a transition in its curvature from circular arc (which forms the throat section) to parabolic contour. At this transition point, the wall contour and wall slope are both continuous, whereas the wall curvature is discontinuous [2]. Further, the parabola is not adapted to the expansion waves coming from the throat (unlike the ideal nozzle design). As a result, compression waves are induced by the parabola leading to formation of an internal shock [2–6]. In Europe, a lot of studies have been carried out to investigate the side-load phenomena in nozzles in the recent past. Of these the most notable contributions have been from Frey [3,6], Frey and Hagemann [2,4-5], Ostlund [6], Terhardt *et al* [8] who observed that the side-loads in a TOP nozzle are associated with conditions of flow transition such as free shock separation (FSS) to restricted shock separation (RSS) and *vice-versa*. The key driver to such flow transitions was found to be the momentum imbalance of flow passing through the overexpansion ( $C_O$ ) and reflected shock ( $C_R$ ), which is initiated by irregular/non-uniform rates of normal shock movement relative to the separation point at different nozzle pressure ratio (NPR). Thereafter lot of studies [9-14] carried out at DLR Lampoldshausen have added valuable information towards side-load generation in this nozzle configuration. The present paper is a continuing effort to further understand these complex flows conditions in such nozzles.

Although lot of studies have been attempted to understand the various flow phenomena in high expansion nozzles, none of these studies focus on the effect of test environment on the flow separation characteristics. The P6.2 subscale cold gas nozzle test facility at DLR Lampoldshausen has the rare luxury of three different nozzle test environments, namely sea-level test stand, high altitude chamber with operation under self-evacuation mode and high altitude chamber with operation using ejector nozzle. The present tests were carried out using a subscale TOP nozzle in the first two test environments. The initial intention was to test the TOP nozzle in the high altitude simulation chamber (HASC) using a subsonic diffuser under self-evacuation mode. Relative to sea-level test results, the flow separation characteristics and the associated side-load activity were observed to change significantly. Surprisingly no restricted shock separation (RSS) condition was observed even with repeated tests. The test model used is the same TOP nozzle used by Frey and Hagemann [2,4-5], Stark [9] and Verma [11-14]. Wall pressure measurements and high-speed schlieren (2kHz) was used to highlight the flow field features.

## II. Experimental Setup and Procedure

### A. Test Facility

Tests were carried out in the cold flow test facility at P6.2 in DLR Lampoldshausen in (i) the horizontal test rig (HTR) with the nozzle exhausting into atmospheric conditions, Fig. 1 (a) and,

(ii) also inside the HASC using a subsonic diffuser, Fig. 1 (b), with nozzle operation under self-evacuation mode (SEM). Gaseous nitrogen at ambient temperature is used as the test gas due to its advantage over compressed air, i.e., the absence of humidity and other impurities that can otherwise cause condensation of flow during nozzle operation.

Figure 2 (a) shows the test nozzle of moderate area ratio (30). The throat diameter of this sub-scale thrust optimized parabolic (TOP) nozzle was 20mm, yielding maximum mass flows in the range of  $m = 4.2 \text{ kg/sec}$ . Fast piezo-resistive pressure sensors (Kulite Semiconductor Inc. model model XT-190M) were used for wall pressure measurement both upstream and downstream of the nozzle throat. Four such pressure sensors are placed in the stagnation chamber and 13 along a single axial line in the supersonic section of the nozzle (with a pitch of 8 mm, sampling frequency 25kHz with a high-pass filter of 8 kHz). Figure 2 (b) shows the choice of axis and the pressure transducer locations for the present tests. The data acquisition system used has the capacity of measuring 64 channels at 1kHz and 16 at 50kHz or 8 at 100kHz.

### III. Results and Discussions

#### A. Streamwise Mean Wall Pressure Distributions

Figures 3 (a) & (b) show the streamwise mean wall pressure distribution for tests in HTR and SEM, respectively during start up operation. The various flow transitions/regimes can be easily identified for the HTR case which have been extensively studied and identified in the past [4-5,9-10,12-14]. In going from NPR 35 to 37 the flow experiences a transition from free-shock separation (FSS) condition to partially formed restricted-shock separation (pRSS) condition which is seen as a significant downstream jump in incipient separation location. The flow remains in pRSS state between NPR 37 to 38 and finally, experiences a pRSS to FSS re-transition wherein the incipient separation location jumps upstream (due to opening of the partially formed separation bubble) [13-14]. Thereafter, the flow enters into the end-effect regime indicated by the lower pressure adaptation to  $P_a$  due to the limited length of back-flow region inside the nozzle [13]. Additionally a small increase in wall static pressure (seen as a bump and marked by an ellipse in Fig. 3 (a)) at  $X/r_t = 8.945$  for  $\text{NPR}=40.87$  and 50 is observed. This is caused due to nitrogen gas condensation at this axial position [15]. It fact the onset of condensation seems to begin for NPR from 36.94 to 40.87 for which a constant value of  $P_w/P_a$  at the separation location is seen. It is well known that the increase in pressure ahead of separation is caused by the release of latent heat of vaporization due to condensation [15-17]. As a result a reduction of Mach number in front of the compression shock occurs resulting in a weaker shock. This effect is known to delay separation in order to maintain the dependence of the shock location with Mach number [16]. Depending upon the initial degree of supersaturation (which is the ratio of vapor pressure to the equilibrium saturation pressure corresponding to the inlet temperature) of test gas and flow Mach number, the shock wave can move either upstream or downstream required pressure recovery. The onset of condensation may also affect the cap-shock location in order to

maintain the pressure recovery to ambient pressure thereby causing it to move slightly upstream. This can shift the momentum balance to favor pRSS condition as is always observed from sea-level tests. Earlier studies [16] also indicate an increased velocity downstream of the shock wave (on condensation) which is related with the source of vapor volume and hence, also diminishes the tendency towards separation. This is because the thermodynamic effects of heat absorption by evaporation affects viscosity which causes flow acceleration and hence counteracts separation [16]. The wall pressure distribution in the present results however do not show such an effect primarily due to the separation moving closer to nozzle exit and also due to occurrence of pRSS condition which partially opens and closes the back-flow region thereby reducing the pressure recovery in this region.

On the other hand, for tests inside HASC, the streamwise mean wall pressure distributions, Fig. 3 (b), reveal only FSS condition at all operating NPR accompanied by a good pressure recovery in the back-flow region indicating the absence of pRSS condition. Up to NPR of 33.5 the incipient separation location shows similar values from both test facilities. However, for  $NPR > 35$  a significant difference in  $X_{inc}/r_t$  location becomes apparent. A careful observation of the wall pressure distributions also indicates the absence of the onset of condensation at any NPR. The wall pressure values at the separation location also show a continuous decrease in its value with increasing NPR. This is primarily caused due to the lower driving pressure ( $P_0$ ) values required inside the HASC to achieve similar NPR (due to the accompanied reduction in  $P_b$  value). Since the gas molecules nucleate at a certain low temperature and high density, a sufficiently low temperature alone may not be enough to trigger the process. As a result a reduction in the gas density (due to reduction in mass flow) prevents the gas to nucleate earlier and hence the process of  $N_2$  condensation is delayed or prevented. As a result the operating test conditions inside HASC alter the flow development process inside the TOP nozzle and hence, favor FSS condition. Similar flow developments may occur when using heated gas for sea-level tests or in hot tests for same TOP nozzle contour.

During shut down, once again completely different conditions are indicated for tests in SEM. Under sea-level tests, shut down sequence always shows a fully formed restricted shock separation (RSS) condition for  $NPR < 35.8$  as seen in Fig. 4 (a), but no RSS condition is observed for tests in SEM, Fig. 4 (b). Figure 5-6 shows the exhaust flow features observed during pRSS and fully formed RSS condition in HTR while Figs. 7-8 show the flow features for similar NPR in HASC. It can be seen that only FSS type of flow condition is apparent at all operating conditions in HASC causing a significant change in the location of incipient separation location.

Figures 9 (a) & (b) show  $X_{inc}/r_t$  movement and the corresponding  $M_{inc}$  variation as a function of NPR in the two test environments. A deviation in the trends from the two test facilities is seen for  $NPR > 33.5$ . While a similar trend in  $X_{inc}/r_t$  vs  $M_{inc}$  is indicated for start up and shut down sequences for tests in HASC, a significant variation can be seen for these sequences from sea-level tests. The latter is caused due to flow transitions from FSS to pRSS & *vice-versa* and FSS to RSS & *vice-versa* [13-14] while the former trend is indicative of the prevalence of FSS condition

at all times. The above observations suggest a strong influence of the test environment on the flow development inside the TOP nozzle. These results should therefore be interpreted with great caution when comparing test results in sea-level and inside high altitude chamber tests.

Although not conclusive at this moment, the primary cause responsible for the observed flow conditions seems to be the reduced mass flow required to attain similar NPR inside a HASC. Any decrease in this value would prevent  $N_2$  condensation (as discussed earlier) and hence, affect the separation location. Absence/onset of condensation may also affect the normal shock location, whose location relative to separation location, is known to control flow transitions in a TOP nozzle [14]. Figure 10 shows schlieren images of the nozzle exhaust flow (NPR=60) for tests in (a) sea-level conditions and, (b) in SEM, for comparison. It can be seen that the test environment significantly affects the exhaust flow structure in a TOP nozzle. The normal shock location for tests in SEM is observed to be downstream of its position in HTR case. Furthermore it can be seen that the angle of the overexpansion shock (shown by white dotted line) under SEM is less than its angle under HTR tests (and hence, suggests a relatively upstream incipient separation location). The lateral distance between the interaction point of overexpansion and reflected shocks is also seen to be much more under SEM. If it is now assumed that the normal shock location for tests in SEM always remains downstream of its position under sea-level tests, then with relatively upstream incipient separation location, the momentum imbalance along overexpansion and reflected shock will favor only FSS condition and hence, flow transitions such as FSS to pRSS or RSS will be prevented.

Figure 11 (a) shows a comparison of the coefficient of thrust ( $C_f$ ) values for start up tests in both facilities. It can be seen that for sea-level tests, the downstream jump in separation results in a sudden drop in nozzle performance after which  $C_f$  begins to recover with increase in NPR or mass flow. This trend is similar to one seen in dual-bell performance where the flow transition from sea-level mode to high-altitude mode shows a drop in value [18] due to drop in momentum thrust. The TOP nozzle performance in HASC however shows a continuous increase indicating absence of any flow transition, as discussed. Figure 11 (b) shows a comparison of the maximum  $rms$  value (of pressure signal from the intermittent region of flow separation) at each NPR for both start up and shut down sequences and for tests in both facilities. It can be seen that the  $rms$  values are significantly different and show much higher values for tests in SEM (even with the prevalent FSS flow condition). This suggests highly fluctuating exhaust flow conditions for tests inside HASC which needs to be investigated.

### B. Side-load signal

A comparison of the strain gauge signal for transient tests from both test facilities also suggests significant changes in the flow structure development inside the TOP nozzle, Figs. 12 and 13. The two peaks indicating the transition from FSS $\rightarrow$ pRSS and *vice-versa* during start up transient in sea-level tests, Fig. 12 (a), are now replaced by a single peak suggesting the absence of FSS $\rightarrow$ pRSS and *vice-versa* flow phenomena in SEM. The range of NPR over which the strain gauge signal shows an increase in value is higher for tests in HASC. The end-effect regime is

seen to occur at NPR or 49 for SEM which for HRT occurs at NPR of 39. Similarly during shut down transient, the strain gauge signal in HTR gradually shows an increase in its amplitude indicating the gradual onset of transition from FSS $\rightarrow$ pRSS. But in SEM, there is a sudden increase in strain gauge signal at  $NPR=42.75$  after which the signal shows a gradual decrease in value. The NPR range over which the strain gauge signal remains high is once again larger for tests in HASC. Further no distinct peaks suggesting the formation and opening of separation bubbles is seen.

An additional feature that needs to be brought forward for tests in HASC is the interaction between the exhaust flow and the diffuser. It can be seen that in between the dominant range during which the strain gauge signal remains high there exists an NPR range in which the strain gauge signal is very weak suggesting stable flow conditions in the nozzle, Fig. 12 (a). However, for tests in HASC, this NPR range shows an overall increase in strain gauge signal suggesting some external influence on the nozzle exhaust flow. Figures 14 and 15 show the exhaust flow from the TOP nozzle for nozzle tests in HTR and SEM, respectively. Each sequence of events is separated by time duration of 0.5ms and direction of events is from left to right. For tests in SEM, the movement of the ring of overexpansion and reflected shock interaction points is marked by a white dotted line with its movement traced in each sequence, Fig. 15. While a very stable exhaust flow can be seen for sea-level test conditions the exhaust flow is seen to considerably fluctuate in its lateral direction when tested in SEM. This interaction gradually reduces as the separation location moves closer to the nozzle exit. The traces of this interaction are also apparent from the strain gauge signals from the bending tube, Fig. 13 (a). It can be seen that up to the beginning of the end-effect regime, the interaction of the exhaust flow with the diffuser produces significant fluctuations in the signal (interference effects), Fig. 13 (b) while very stable flow conditions can be observed for sea-level test signals, Fig. 12 (a). It may also be pointed out that the NPR range over which the TOP nozzle operation is discussed, the diffuser is not working in the start mode and hence, can significantly affect the stable nozzle flow operation. These interference effects therefore need to be investigated in detail and their effects on nozzle flow and its subsequent interpretation should be dealt with caution.

#### IV. Conclusions

An experimental investigation has been carried out to study the flow separation characteristics of a TOP nozzle in two different test environments, namely (i) sea-level conditions with the nozzle exhausting into atmosphere and, (ii) inside a HASC with the nozzle operation under SEM. It is observed that the normal shock location for tests in SEM is observed to be downstream of its position in sea-level case and the angle of the overexpansion shock under SEM is less than its angle under sea-level tests. The incipient separation location in SEM is found to be considerably upstream of its location under sea-level tests. The above causes the momentum imbalance along the overexpansion and reflected shocks to only favor FSS condition (both during start up and shut down) and hence, flow transitions such as FSS to pRSS or RSS and *vice-versa* are totally prevented. Although not conclusive at this moment, the primary cause responsible for the observed flow conditions seems to be the reduced mass flow required to attain similar NPR inside

a HASC which prevents nitrogen condensation and hence, affects the flow development inside a TOP nozzle. Both the unsteady wall pressure analysis and side-load signals before the end-effect regime shows significant interference effects between the nozzle exhaust and the diffuser. As a result, extreme caution should be exercised while interpreting test results from HASC.

### Acknowledgements

The results reported in this paper are from the work carried out by the first author during his 3 month tenure under resumption of Humboldt fellowship at Space Propulsion Institute, DLR Lampoldshausen, Germany between May to July 2007. The author would like to thank Dr. Ralf Stark and Bernd Wagner for the useful discussions and Herr Christian Boehm for his immense help during the entire course of the experiments.

### References

- [1] L.H. Nave and G.A. Coffey, ``Sea level side loads in high-area-ratio rocket engines'', AIAA Paper 73-1284, *AIAA/SAE 9th Propulsion Conference*, Las Vegas, Neveda, 1973.
- [2] Frey, M., and Hagemann, G., "Status of Flow Separation Prediction in Rocket Nozzles," AIAA Paper 98-3619, 1998.
- [3] Frey, M., ``Shock Patterns in the Exhaust Plume of Rocket Nozzles'', *Proceedings of the 3rd European Symposium on Aerothermodynamics of Space Vehicles*, pages 395--403, ESA-ESTEC, Noordwijk, The Netherlands, 1998.
- [4] Frey, M. and Hagemann, G, ``Restricted Shock Separation in Rocket Nozzles'', *Journal of Propulsion and Power*, 16(3): pp. 478--484, 2000.
- [5] Frey,M. and Hagemann,G.,``Flow Separation and Side-Loads in Rocket Nozzles'', AIAA-99-2815
- [6] Frey, *Behandlung von Stroemungsproblemen in Raketen bei Ueberexpansion*, Ph.D thesis, Institut fuer Aerodynamik und Gasdynamik, Universitaet Stuttgart, 2000, Germany.
- [7] Oestlund, J., Damgaard, T., and Frey, M., "Side-Load Phenomena in Highly Overexpanded Rocket Nozzles," *Journal of Propulsion and Power*, Vol. 20, No. 4, 2004,
- [8] Terhardt, M. , Hagemann, G. and Frey, M., ``Flow Separation and Side-Load Behaviour in the Vulcain Engine'', AIAA 99-2762.
- [9] Stark, R., Kwan, W., Quessard, F., Hagemann, G. And Terhardt, M., ``Rocket Nozzle Cold-Gas Test Campaigns for Plume Investigations'', 4<sup>th</sup> European Symposium on Aerothermodynamics for Space Vehicles, Capua, Italy, Oct. 15-18, 2001.
- [10] Kwan, W. and Stark, R., ``Flow Separation Phenomena in Subscale Rocket Nozzles'', AIAA-2002-4229.
- [11] Gross, A., Haidn O., Stark R., Zeiss, W., Weber C., and Weiland, C., ``Experimental and numerical investigation of heat loads in separated nozzle flow'', AIAA 2001-3682.
- [12] Verma, S. B., Stark, R., and Haidn, O., "Relation Between Shock Unsteadiness and the Origin of Side-Loads in a Thrust Optimized Parabolic Rocket Nozzle," *Aerospace Science and Technology*, Vol. 10, No. 6, Aug. 2006.

- [13] Verma, S.B., ``Shock Unsteadiness in a Thrust Optimized Parabolic Rocket Nozzle'', *Journal of Shock Waves, Detonations and Explosions*, Invited paper for the special Issue on Nozzle Flow Separation, Volume 19, Issue 3 (2009), Page 193-212.
- [14] Verma, S.B. and Haidn, O., ``Study on Restricted Shock Separation Phenomena in a Thrust Optimized Parabolic (TOP) Nozzle'', *AIAA Journal of Propulsion and Power*, Vol. 25, No.5, Sept-Oct. 2009, pp. 1046-1057.
- [15] Okada, Y., Sunouchi, K., Ryu, H., Patra, A., Ashmine, K. And Takeuchi, K., ``Measurement of Condensation Onset in Steady Supersonic Laval Nozzle Flow for the Molecular Laser Isotope Separation Process'', *Journal of Nuclear Science and Technology*, 1998, Vol. 35, No. 2, pp. 158-162.
- [16] Doeffer, P., Szumowski, A. and Yu, S., ``The effect of Air Humidity on Shock Wave Induced Incipient Separation'', *Journal of Thermal Science*, 2000, Vol. 9, No.1, pp. 45-50
- [17] Setoguchi, T. and Matsuo, S., ``Effect of Non-Equilibrium Homogenous Condensation on Flow Fields in a Supersonic Nozzle'', *Journal of Thermal Science*, 1996, Vol. 6, No.2, pp. 90-96
- [18] Verma, S.B., Stark, R., Genin, C. and Haidn, O., ``Flow Separation Characteristics of a Dual-Bell Nozzle during its Transition Modes'', *Journal of Shock Waves*, Vol. 20, Issue 3, June 2010, pp. 191-203.

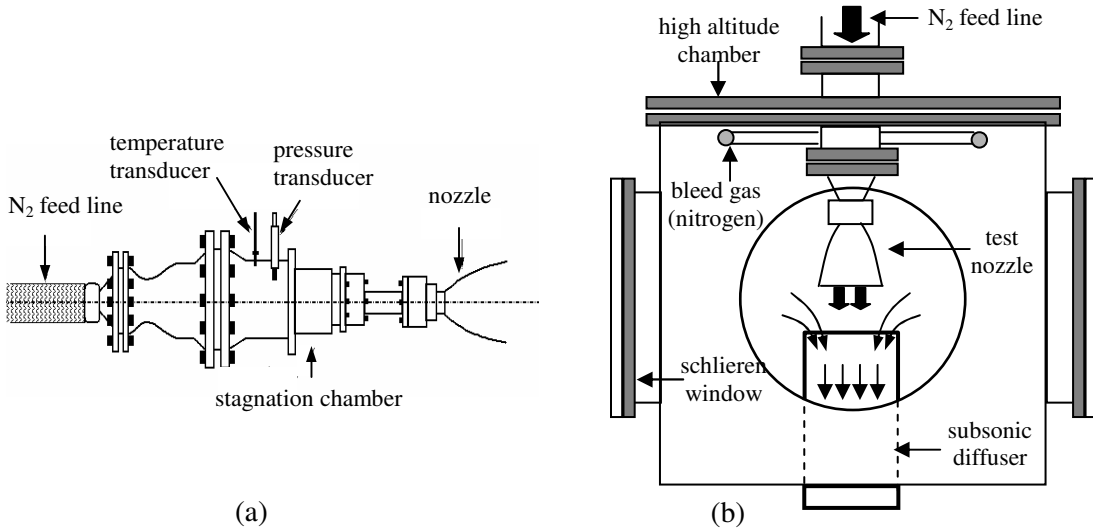


**Figure 1:** (a) Schematic of the horizontal nozzle test-facility (sea-level runs) and (b) schematic of the high altitude simulation chamber (HASC) nozzle test-facility

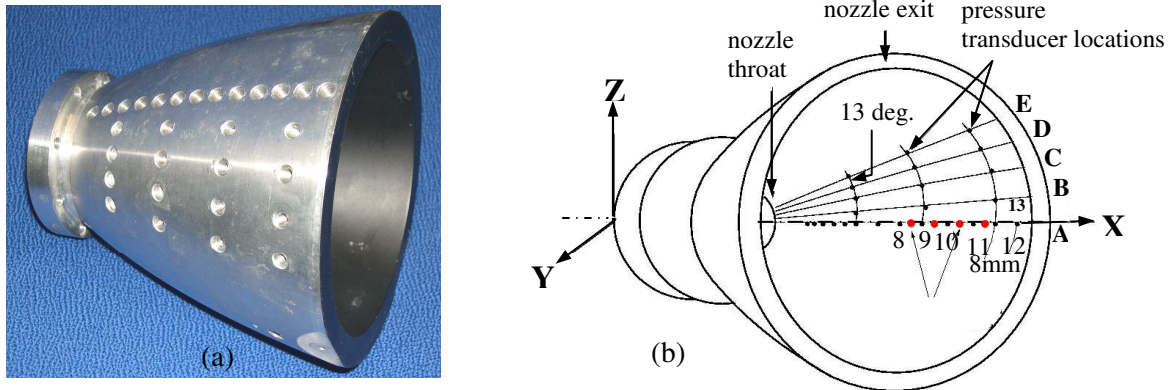


**Figure 2:** (a) Picture of the thrust optimized parabolic test nozzle and, (b) schematic of the pressure sensor locations and the choice of axis

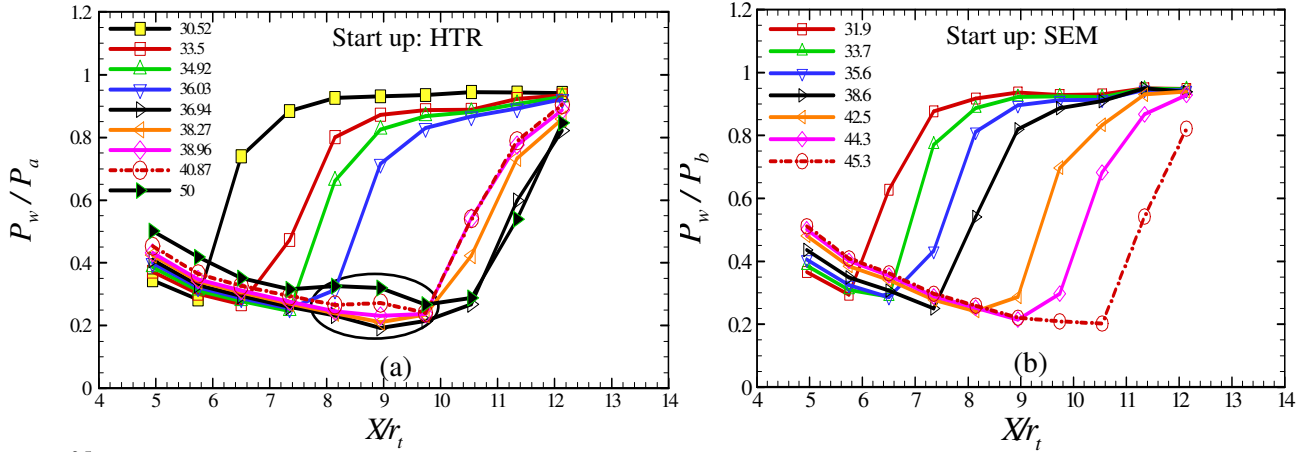


**Figure 3:** Mean wall pressure distribution in a thrust optimized parabolic nozzle during start up sequence for tests in (a) sea-level conditions and, (b) a HASC with subsonic diffuser

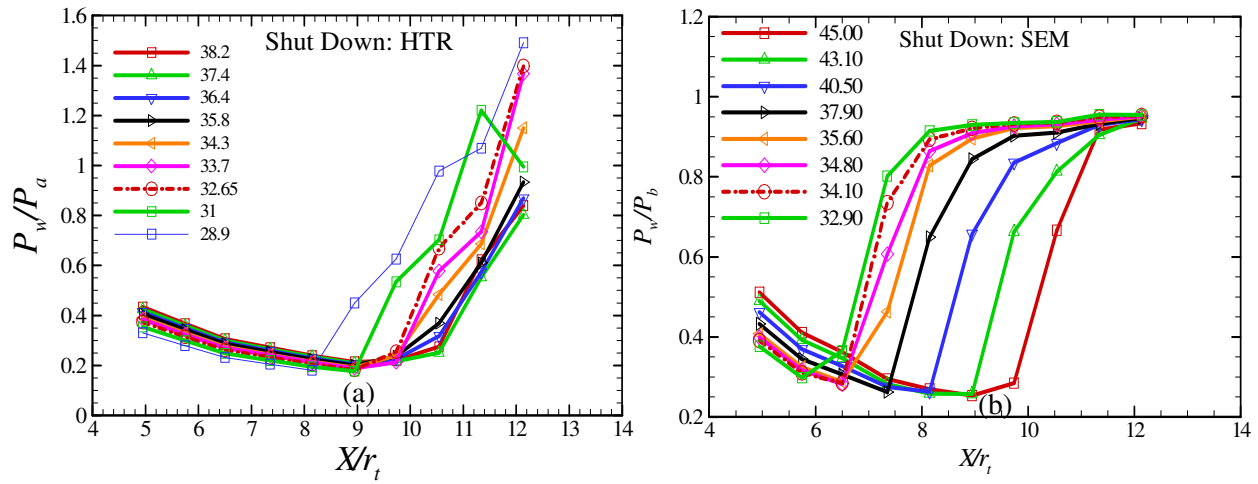


**Figure 4:** Mean wall pressure distribution in a thrust optimized parabolic nozzle during shut down sequence for tests in (a) sea-level conditions and, (b) HASC with a subsonic diffuser

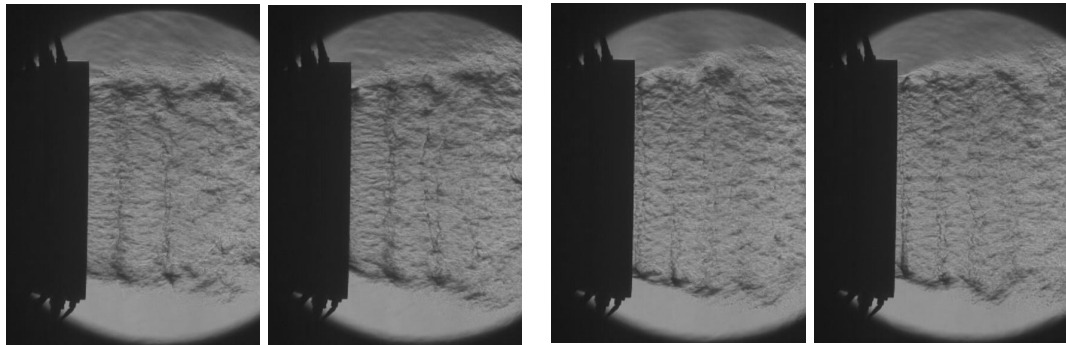


**Figure 5:** NPR=38.2 shut down sequence in HTR; **Figure 6:** NPR=32.65 shut down sequence in HTR; RSS pRSS

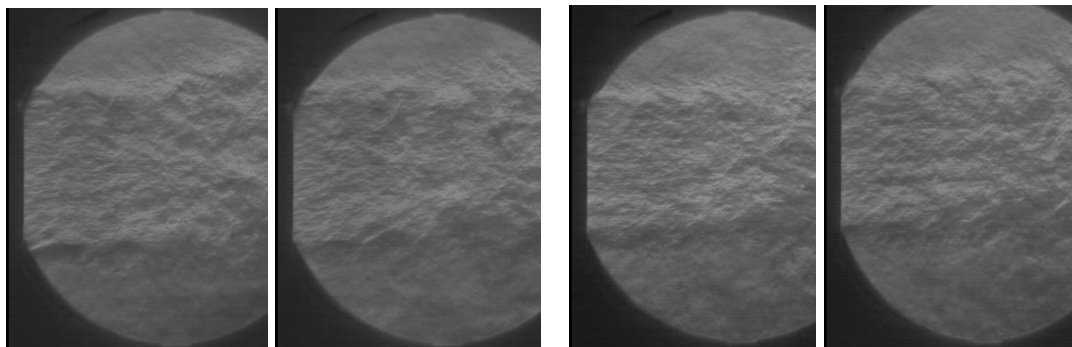


**Figure 7:** NPR=37.9 shut down sequence in SEM; FSS **Figure 8:** NPR=32.9 shut down sequence in SEM; FSS

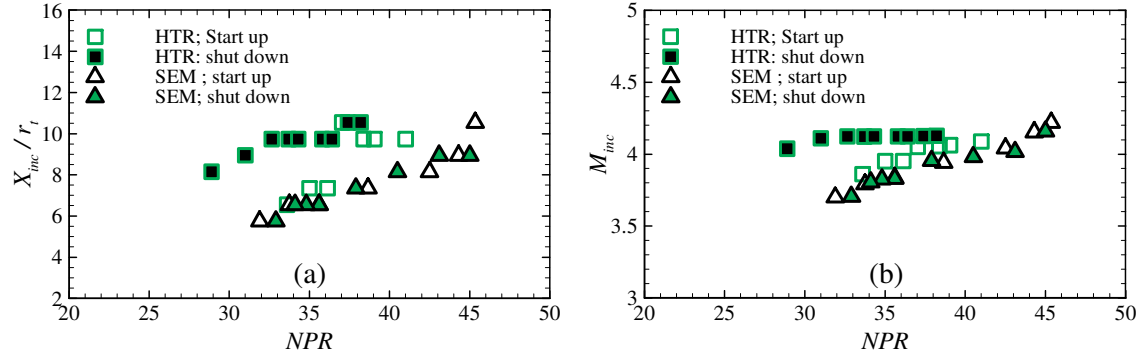


**Figure 9:** Comparison of data for tests in the two facilities showing (a) incipient separation location and, (b) incipient separation Mach number variations

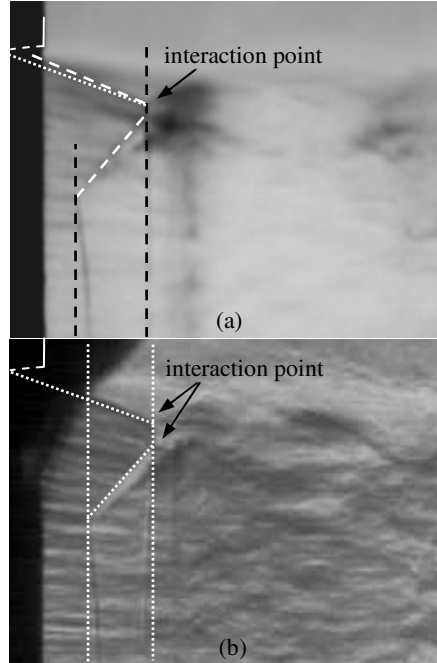


**Figure 10:** Comparison of schlieren pictures of the exhaust flow from the TOP nozzle for tests in (a) sea-level conditions and, (b) SEM;  $NPR=60$

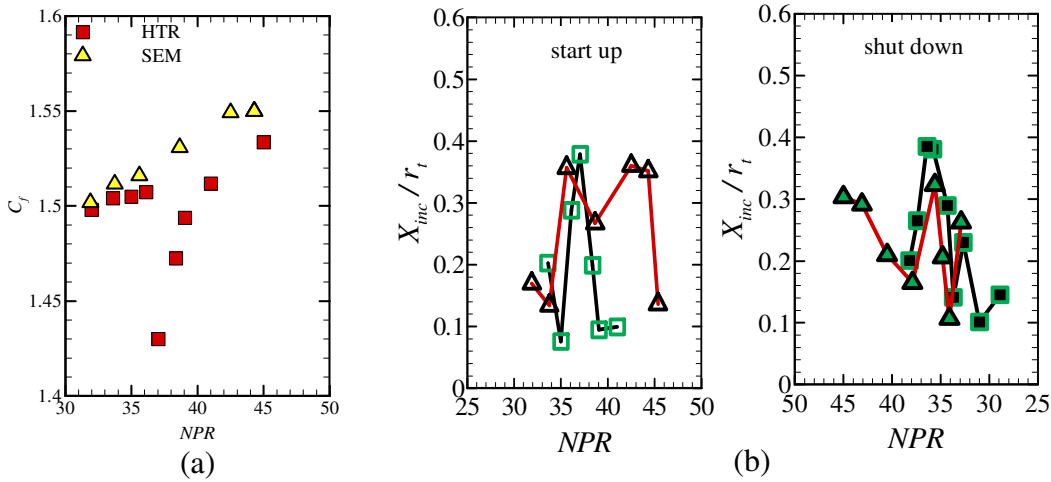


**Figure 11:** Comparison of (a) nozzle performance in the two test facilities and, (b) maximum *rms* data for tests in the two facilities during start up and shut down; square symbol are for tests in HTR and delta symbol for test in SEM

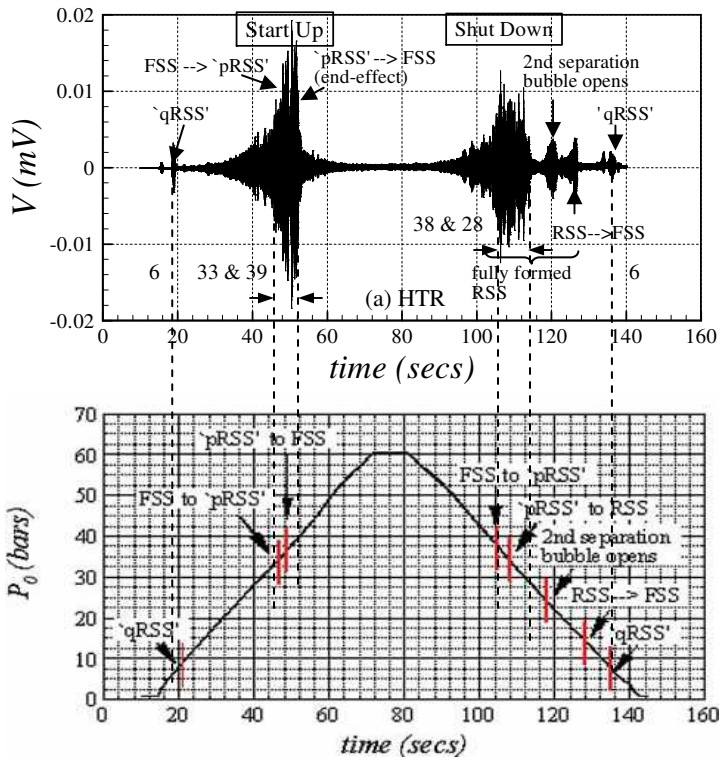


**Fig. 12:** Strain gauge signal in XY-direction for tests in HTR showing the appearance of peaks during start up and shut down transients.

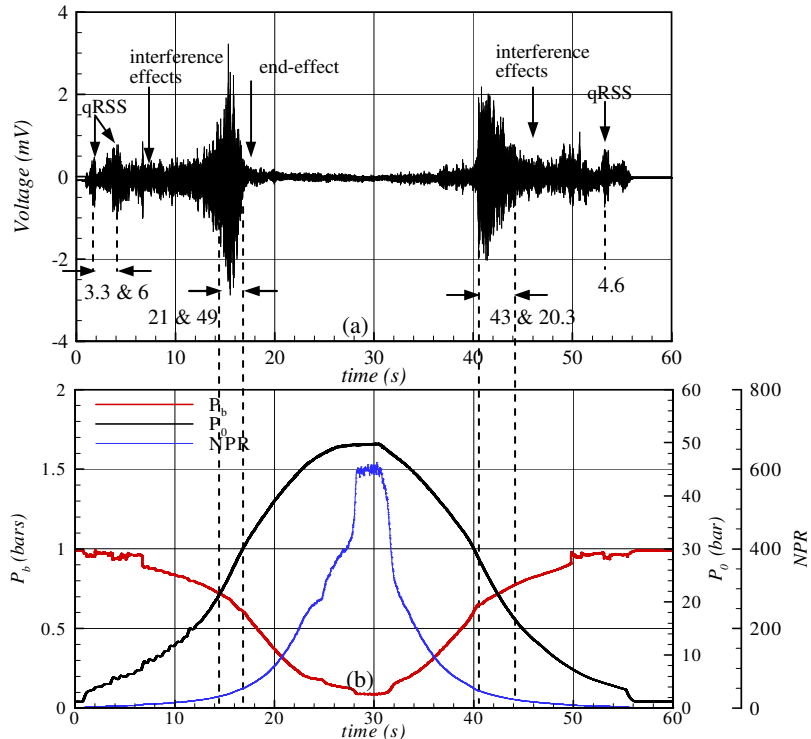


**Fig. 13:** Strain gauge signal in XY-direction from one of the tests in HASC operating in SEM showing the appearance of peaks during start up and shut down transients.

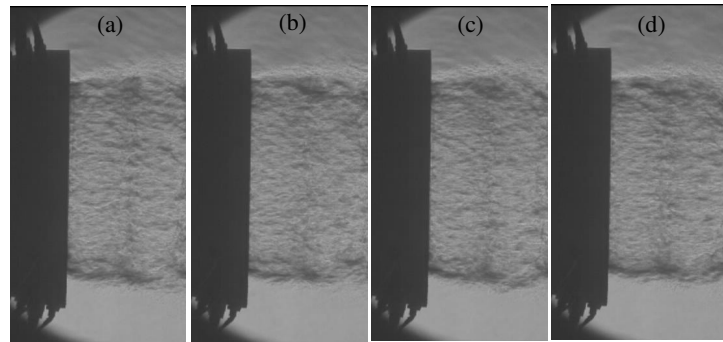


**Figure 14:** Schlieren pictures using high-speed camera (2kHz); each event is separated by a time duration of 0.5ms; NPR=41 start up sequence in HTR

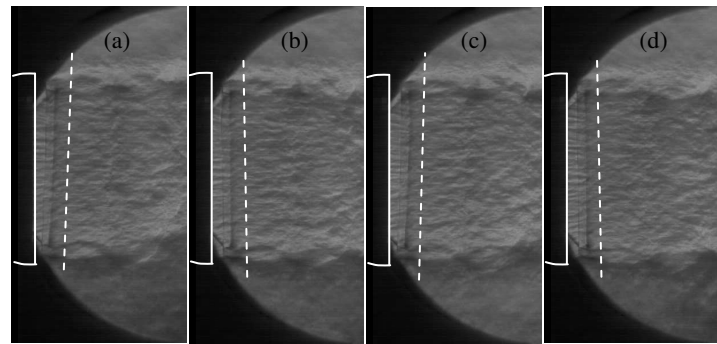


**Figure 15:** Schlieren pictures using high-speed camera (2kHz); each event is separated by a time duration of 0.5ms; NPR=45.3 start up sequence in SEM